

Article

Optimal Calibration of an Adaptive and Predictive Energy Management Strategy for Fuel Cell Electric Trucks

Alessandro Ferrara ^{1,*}, Saeid Zendegan ¹, Hans-Michael Koegeler ², Sajin Gopi ², Martin Huber ³, Johannes Pell ³ and Christoph Hametner ^{1,4}

¹ Institute of Mechanics and Mechatronics, Division of Process Control and Automation, TU Wien, 1060 Vienna, Austria; saeid.zendegan@tuwien.ac.at (S.Z.); christoph.hametner@tuwien.ac.at (C.H.)

² AVL List GmbH, 8020 Graz, Austria; hans-michael.koegeler@avl.com (H.-M.K.); sajin.gopi@avl.com (S.G.)

³ AVL List GmbH, 4407 Steyr, Austria; martin.huber@avl.com (M.H.); johannes.pell@avl.com (J.P.)

⁴ Christian Doppler Laboratory for Innovative Control and Monitoring of Automotive Powertrain Systems, TU Wien, 1060 Vienna, Austria

* Correspondence: alessandro.ferrara@tuwien.ac.at

Abstract: Energy management strategies have a significant impact on the hydrogen economy of fuel cell trucks and the lifetime of battery and fuel cell systems. This contribution presents the design and optimal calibration of an energy management strategy that is adaptive to the battery and ambient temperatures. Indeed, fuel cell trucks face critical operating conditions due to high ambient temperatures or high loads on long uphill roads. However, the presented adaptive energy management strategy shifts the electric loads to the fuel cell system to limit the battery usage, avoiding accelerated degradation due to battery temperature peaks without hindering the hydrogen economy. The strategy design and calibration involves a multi-objective optimization of performance indicators related to hydrogen consumption, fuel cell degradation, battery thermal state, equivalent charge/discharge cycles, and charge control. This work uses AVL CAMEO to systematically vary the adaptive curve parameters to explore the trade-off between the key performance indicators. The calibration considers real-world driving cycles of road freight vehicles, including measured speed, road elevation, and variable vehicle mass. Moreover, the energy management design is robust because the performance indicators are evaluated over 8935 km, covering an extensive range of real-world driving scenarios. Eventually, the adaptive and predictive energy management strategy proposed in this work can meet all the performance targets thanks to the optimal calibration, and it is particularly effective in avoiding battery temperature peaks.

Keywords: energy management strategy; fuel cell truck; optimal calibration; adaptive control; battery temperature; fuel cell degradation; battery thermal management



Citation: Ferrara, A.; Zendegan, S.; Koegeler, H.-M.; Gopi, S.; Huber, M.; Pell, J.; Hametner, C. Optimal Calibration of an Adaptive and Predictive Energy Management Strategy for Fuel Cell Electric Trucks. *Energies* **2022**, *15*, 2394. <https://doi.org/10.3390/en15072394>

Academic Editors: Zachary D. Asher and Thomas H. Bradley

Received: 15 February 2022

Accepted: 22 March 2022

Published: 24 March 2022

Publisher's Note: MDPI stays neutral with regard to jurisdictional claims in published maps and institutional affiliations.



Copyright: © 2022 by the authors. Licensee MDPI, Basel, Switzerland. This article is an open access article distributed under the terms and conditions of the Creative Commons Attribution (CC BY) license (<https://creativecommons.org/licenses/by/4.0/>).

1. Introduction

Fuel cells are considered more appealing than batteries as the primary energy source of heavy-duty electric vehicles due to the high power and range requirements [1–3]. In particular, the most feasible and promising application is for fuel cell electric trucks for road freight transports, which have sufficient space for hydrogen storage tanks under the side rails, behind the cab, and under the chassis to cover their daily operation range [4].

Supervisory control is a critical function in heavy-duty fuel cell vehicles because it highly affects their operating costs and powertrain components lifespan. In particular, the energy management system operates the power-split of the electric load demand between the fuel cell and battery systems with the targets of low hydrogen consumption, limited fuel cell degradation, and suitable battery state-of-charge (SoC) control to avoid accelerated degradation [5]. At the same time, the thermal management system ensures that the powertrain components are operated in a suitable temperature range to avoid accelerated

degradation. Therefore, developing optimal energy and thermal management strategies can significantly contribute to the advancement of heavy-duty fuel cell vehicles.

Energy management strategies (EMSs) have been largely investigated for different hybrid electric vehicle topologies and applications, considering various targets for the definition of the control design criteria [6–9]. The design of EMSs for fuel cell battery vehicles is described in [10–30]. The predictive energy management of heavy-duty fuel cell vehicles for road freight transports has been investigated in [5,31,32] to find a suitable trade-off between fuel consumption and powertrain components degradation. In particular, it was shown that predictive EMSs are highly beneficial to control the SoC operating range and depth-of-discharge for trucks driving in mountain routes. Some studies have been conducted to investigate the interaction between energy and thermal management, including the maximum battery temperature constraints within the power-split optimization problem [33,34]. Indeed, avoiding battery temperature peaks is essential to prevent accelerated system degradation and thermal runaways that can cause fires or explosions [35–37].

This paper focuses on the optimal calibration of an adaptive and predictive energy management strategy for fuel cell electric trucks using AVL CAMEO. The study adopts the predictive energy management system described in [31], proposing an improved formulation to avoid battery temperature peaks. In particular, the control strategy adapts to the battery and ambient temperatures, shifting the electric loads to the fuel cell system (FCS) to limit the battery usage in critical conditions and avoid temperature peaks. The adaptive control is implemented using optimally calibrated maps to adjust the main control parameters depending on the ambient and battery temperatures. The parameter maps are calibrated using AVL CAMEO considering the trade-off between hydrogen consumption, fuel cell voltage degradation, maximum battery temperature, equivalent battery charge/discharge cycles, and SoC control. Realistic driving simulations show that temperature peaks over 47 °C (considered the threshold for accelerated battery degradation) are effectively avoided for 32 selected real-world driving cycles and ambient temperatures between 5 °C and 35 °C. Eventually, the benefits of the adaptive and predictive EMS are evaluated by comparing the performance with non-adaptive and non-predictive strategies.

The remainder of this paper is structured as follows. Section 2 outlines the simulation framework for the performance evaluation of fuel cell electric trucks in realistic driving scenarios. Section 3 describes the adaptive and predictive energy management system, and the optimal calibration process using AVL CAMEO. Section 4 analyses the simulation results of fuel cell truck performance and compares different strategies to highlight the benefits of the proposed method.

2. Performance of Fuel Cell Electric Trucks in Realistic Driving Simulations

This study evaluates the performance of fuel cell electric trucks in realistic driving scenarios adopting the simulation framework developed within the Austrian research projects HyTruck [38] and FC4HD [39]. An overall description of the simulation model structure and main components is presented below to provide a good understanding of the key performance indicators under investigation for optimal energy management design. On the other hand, detailed modeling of the individual vehicle components is beyond the scope of the paper.

2.1. Fuel Cell Vehicle Modeling

The simulation model is developed in MATLAB/Simulink, and its overall structure is depicted in Figure 1. A fixed-step solver is adopted with a sample time of 200 ms. The modeling approach is forward-facing, meaning that there is a driver model that creates a power demand to follow a specific driving cycle. If the fuel cell and battery systems do not provide the load demand, the vehicle slows down. In particular, the driver model defines desired electric load depending on the road slope and the deviation between actual and desired speed:

$$P_{el,des} = f(\alpha, v, v_{des}) . \quad (1)$$

The model consists of a PI controller that creates the load demand based on the deviation between actual and desired speed, which is a classical approach in the literature [40]. Additionally, the road slope is used to create a feedforward term to improve the tracking of the desired speed.

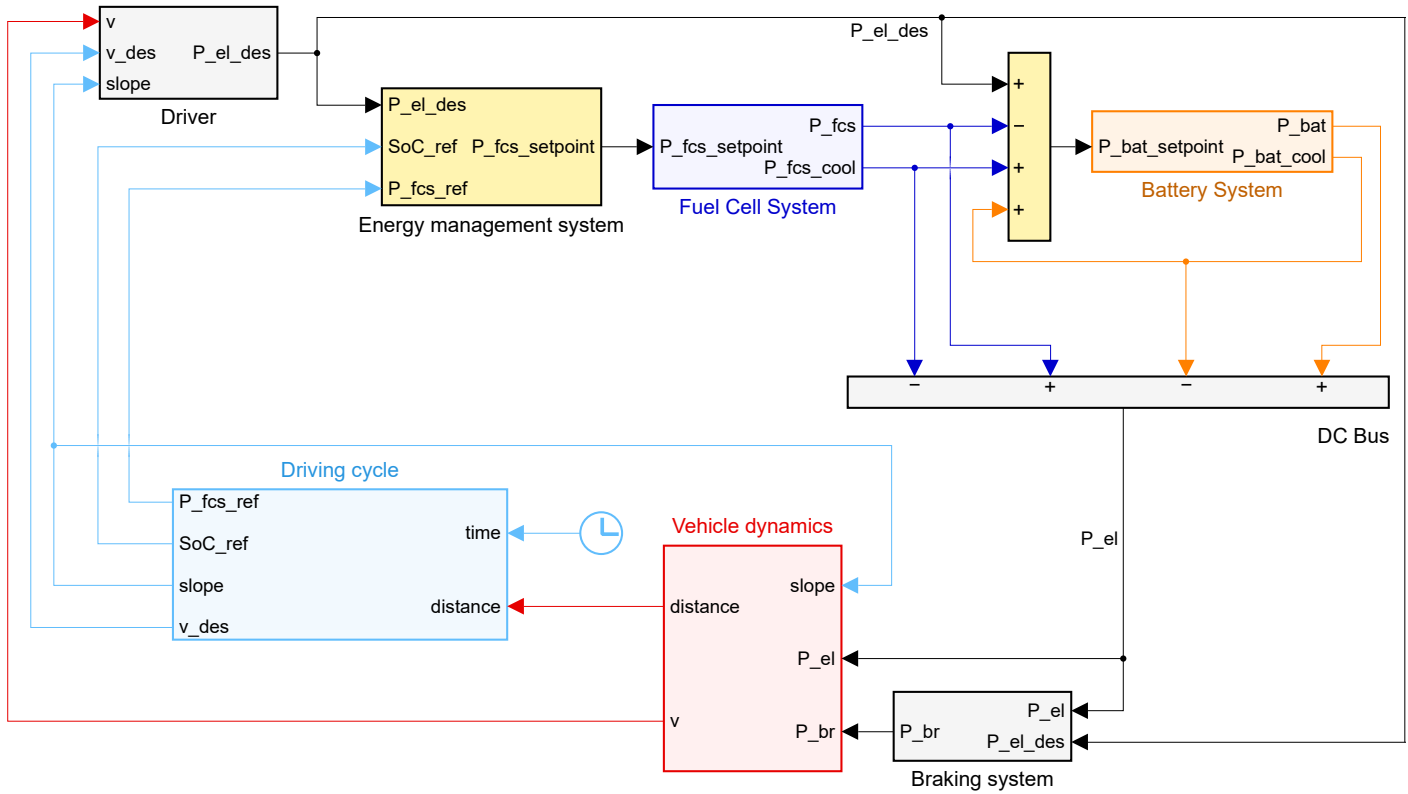


Figure 1. Overview of the fuel cell vehicle model in MATLAB/Simulink. For readability, some signals are hidden and exchanged directly between subsystems.

The energy management system performs the power-split by defining the fuel cell setpoint using the adaptive and predictive strategy detailed in Section 3. On the other hand, the battery setpoint is defined to buffer the fuel cell operation, compensating for the remaining part of the desired load and the electric losses of the cooling systems. Eventually, the electric power on the DC bus is calculated as the sum of fuel cell and battery power minus the electric losses of the cooling systems:

$$P_{el} = P_{fcs} + P_{bat} - P_{fcs,cool} - P_{bat,cool} . \quad (2)$$

The fuel cell and battery systems are subject to the power constraints expressed in (3)–(5), which hinder the exact following of the setpoints defined by the EMS. In particular, the battery power restrictions derive from the cell voltage and C-rate limits to avoid accelerated degradation. Since the battery characteristics change depending on the operating conditions, these constraints depend on SoC and temperature.

$$0 \leq P_{fcs} \leq P_{fcs,nom} \quad (3)$$

$$|\dot{P}_{fcs}| \leq 0.10 \cdot P_{fcs,nom} \quad (4)$$

$$P_{bat,min}(SoC, T_{bat}) \leq P_{bat} \leq P_{bat,max}(SoC, T_{bat}) \quad (5)$$

Using an equivalent circuit model of the battery system, the SoC rate of change is calculated depending on the battery power as:

$$\dot{SoC} = -\frac{V_{oc} - \sqrt{V_{oc}^2 - 4 P_{bat} R_{int}}}{2 Q_{bat,nom} R_{int}} \quad (6)$$

where the open-circuit voltage V_{oc} and internal resistance R_{int} depend on SoC and temperature, and the nominal charge $Q_{bat,nom}$ is constant.

The fuel cell cooling system includes an electric fan to dissipate the radiator heat. The operation and energy consumption of the electric fan depend on the vehicle speed, ambient temperature, and fuel cell heat generation:

$$P_{fcs,cool} = f(v, T_{amb}, P_{fcs}) . \quad (7)$$

The battery cooling system consists of a chiller system, two cooling circuits (with oil and coolant), and three heat exchangers (battery/oil, oil/coolant, and coolant/chiller). In the primary circuit, the oil absorbs the battery pack heat through liquid cooling plates. Then, the oil dissipates the heat with the coolant through a counterflow heat exchanger. Lastly, in the secondary circuit, the coolant is cooled down by the chiller system. A hysteresis controller regulates the chiller operation depending on the battery temperature, switching the system on at 40 °C and off at 35 °C. The coefficient of performance (COP) of the cooling system depends on the ambient temperature and chiller cooling power, including the losses of its main components (i.e., compressor and coolant pump). Therefore, the electric losses of the cooling system are expressed as:

$$P_{bat,cool} = \dot{Q}_{chill} / COP(T_{amb}, \dot{Q}_{chill}) . \quad (8)$$

The electric motor power is calculated considering the auxiliary loads that are external to the powertrain (e.g., cabin conditioning, power-steering pump) as follows:

$$P_m = P_{el} - P_{aux} . \quad (9)$$

The power at wheels is determined depending on the electric motor and mechanical braking power as:

$$P_w = P_m \eta_T^{\text{sgn}(P_m)} - P_{br} , \quad (10)$$

where η_T is the total efficiency of electric motors, inverters, and drivetrain components. The mechanical braking system absorbs the negative loads that cannot be regenerated by the electric motor due to the battery power constraints. Eventually, the vehicle acceleration is calculated as:

$$\dot{v} = \frac{P_w/v - F_{res}(v, \alpha)}{m_v} , \quad (11)$$

where the resistant force consider the aerodynamic drag, the road slope, and the wheels rolling friction, as in [32].

The simulation results of a real-world driving cycle are depicted in Figure 2 in terms of speed, elevation, fuel cell power, battery power, electric power for fuel cell and battery cooling, SoC, and battery, oil, and coolant temperatures. The results provide a general overview of the main challenges that fuel cell electric trucks face in long uphill due to the heavy vehicle weight (in this case, 42 tons). In particular, the battery degradation is accelerated due to low SoC levels (at minute 155) and temperature peaks (at minute 110). On the other hand, the fuel cell system operates at high power for a significant time causing high voltage degradation and hydrogen consumption.

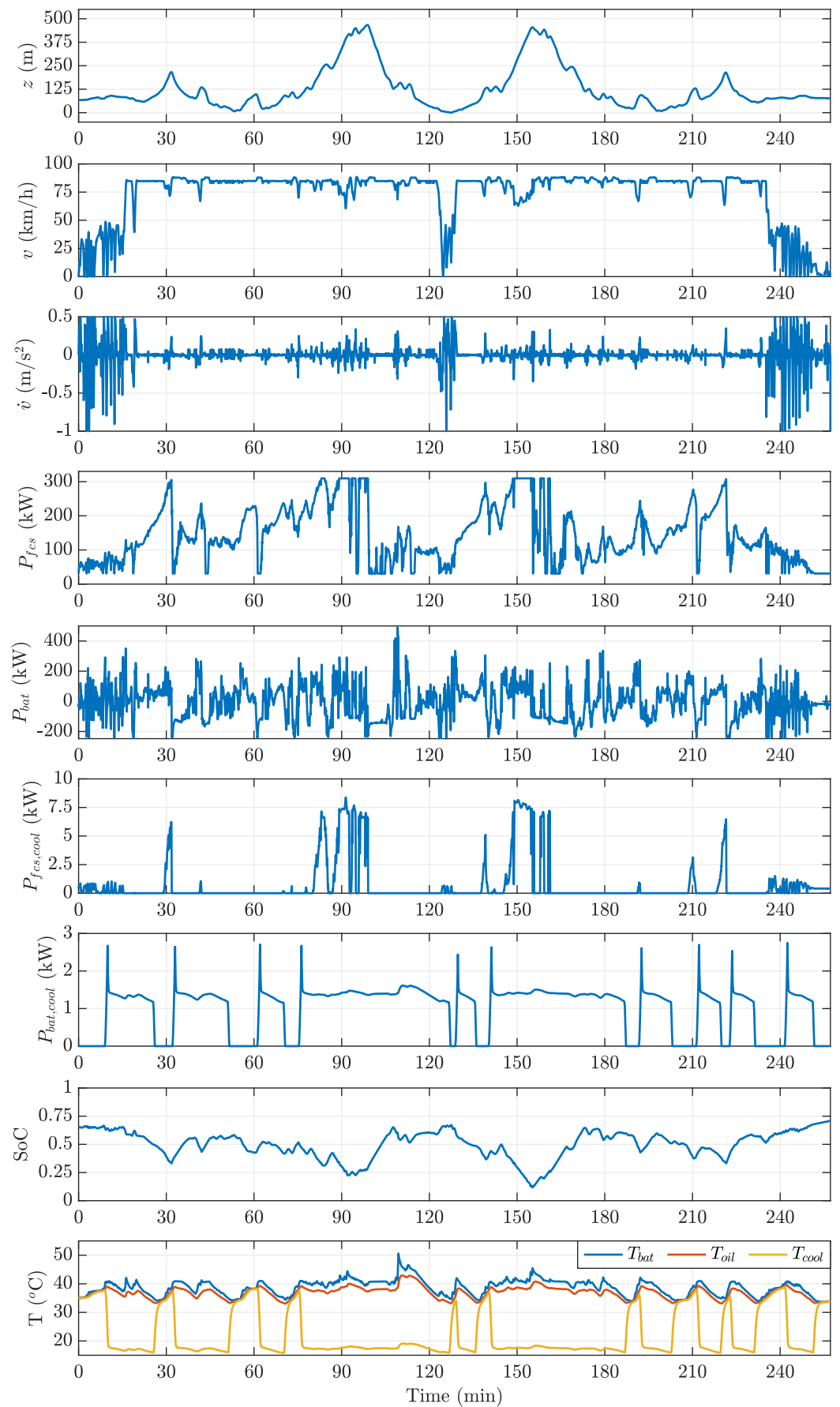


Figure 2. Driving simulation of a fuel cell electric truck (42 tons) in a real-world driving cycle.

2.2. Performance Indicators in Realistic Driving Scenarios

This study considers a multi-objective optimization of hydrogen consumption, fuel cell degradation, battery thermal state, equivalent charge/discharge cycles, and SoC control for the strategy design and calibration. The vehicle performances are evaluated over 8935 km to cover an extensive range of driving scenarios and obtain a robust EMS design. In particular, the simulations consider 32 real-world driving cycles based on speed and road elevation measurements of road freight vehicles operating in Central Europe. Some key driving cycle properties are shown in Figure 3, indicating a significant variety of scenarios. The average speed and traveled distance indicate that the investigation focuses on motorway or rural driving cycles. High relative positive accelerations (RPAs) represent sub-urban driving with traffic and frequent turns, whereas low values represent stable motorway cruising. The vehicle mass ranges between 16 and 42 tons. High total climb indicates long steep roads or frequent ups-and-downs, whereas the difference between maximum and minimum elevation indicates flat, hilly, or mountain roads. The driving cycle in Figure 2 corresponds to the sample number 32 of Figure 3. Moreover, the speed and elevation profile of the driving cycles 1, 5, 9, 18, and 30 are shown in Figure 4.

The total hydrogen consumption is calculated by integrating the consumption rate as follows:

$$m_{H_2} = \int \dot{m}_{H_2} dt . \quad (12)$$

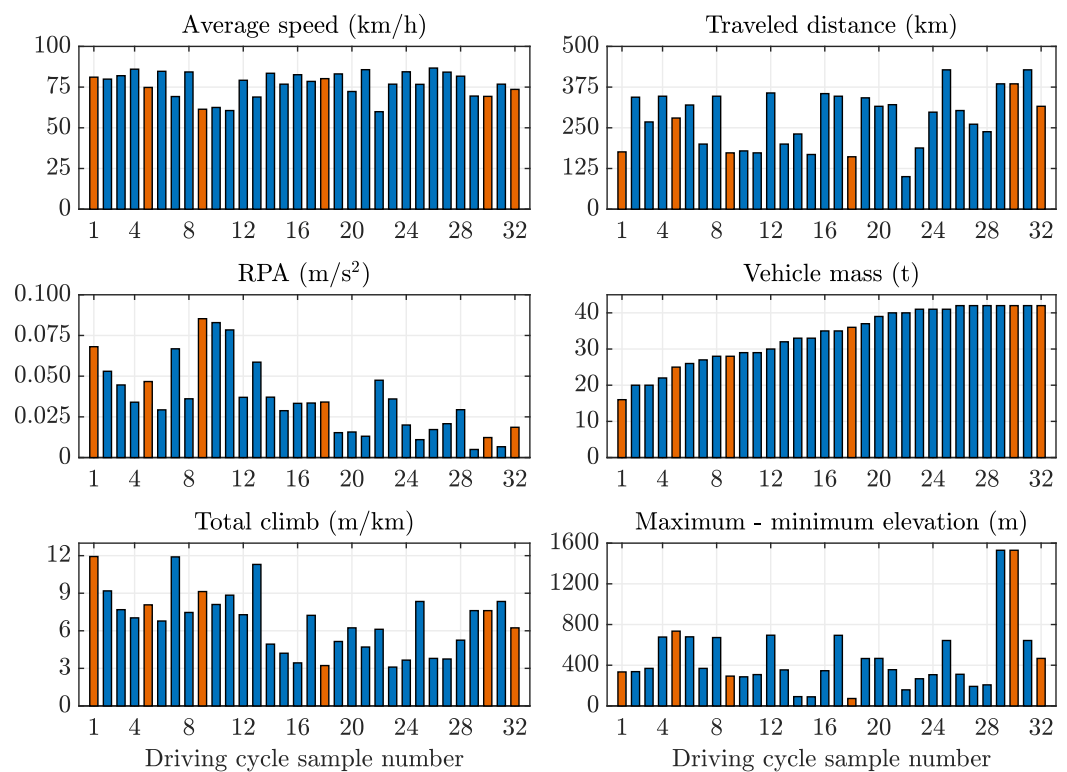


Figure 3. Key properties of the real-world driving cycles under investigation in this work. The cycles are sorted by vehicle mass, which ranges between 16 and 42 tons. In total, the traveled distance is 8935 km and the driving time 116 h.

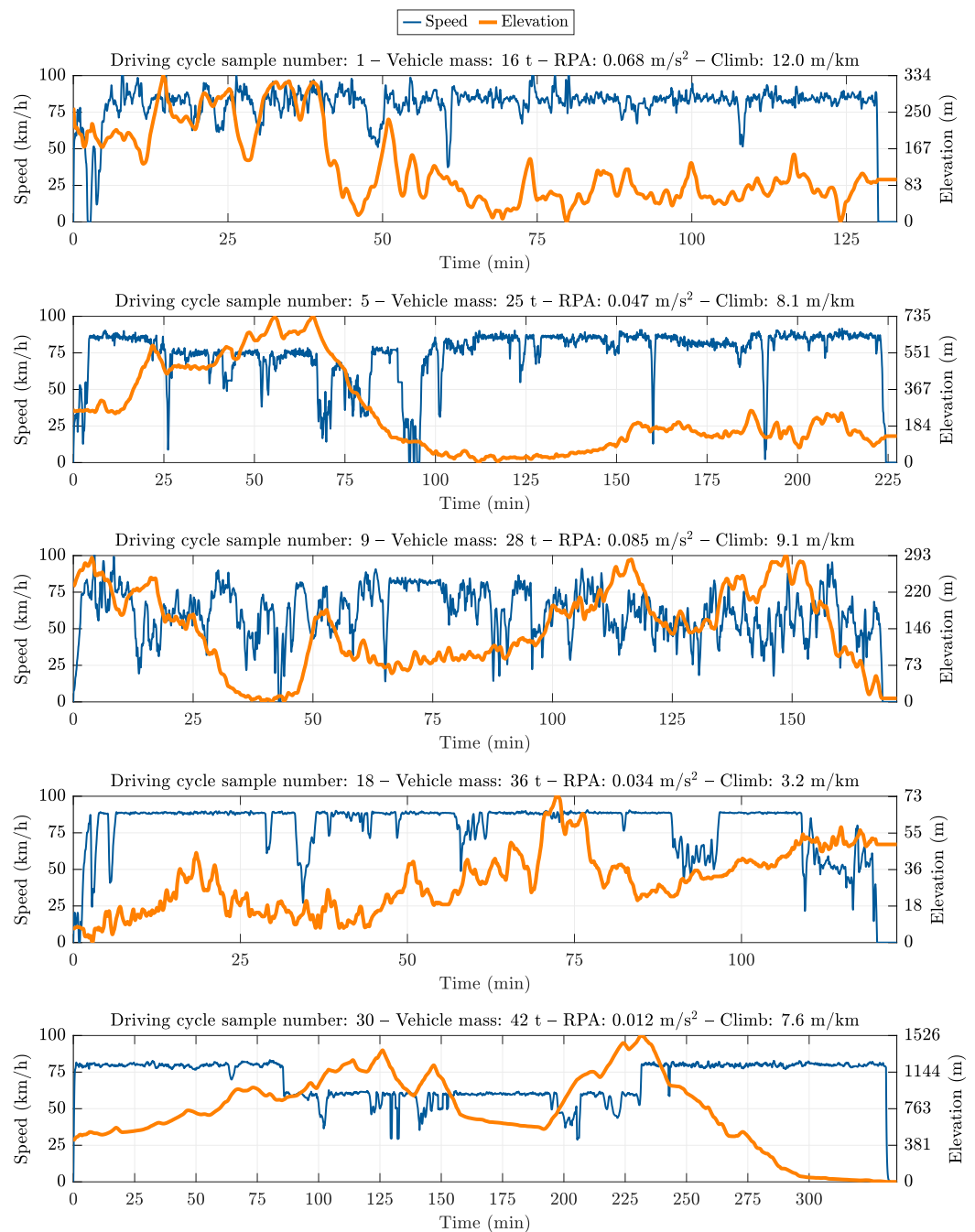


Figure 4. Speed and elevation profiles of five selected real-world driving cycles.

The voltage degradation of the fuel cell system is calculated in (13)–(17), considering start-up/shut-down cycles, low-power operation, high-power operation, and dynamic loading.

$$\Delta V_{fcs} = \Delta V_{fcs,ss} + \Delta V_{fcs,lp} + \Delta V_{fcs,hp} + \Delta V_{fcs,dl} \quad (13)$$

$$\Delta V_{fcs,ss} = 0.00196 \cdot N_{fcs,starts} \quad (14)$$

$$\Delta V_{fcs,lp} = 0.00126 \cdot t_{fcs,lp} \quad (15)$$

$$\Delta V_{fcs,hp} = 0.00147 \cdot t_{fcs,hp} \quad (16)$$

$$\Delta V_{fcs,dl} = 0.0000593 \cdot \int |\dot{P}_{fcs} / P_{fcs,nom} / 2| dt \quad (17)$$

This quick evaluation method derives from accelerated aging tests and offers adequate precision for a system level analysis [41]. The number of fuel cell starts $N_{fcs,starts}$ is always 1,

assuming that the FCS only shuts down at the end of the driving cycle. The thresholds for low and high-power operation to calculate the time intervals $t_{fcs,lp}$ and $t_{fcs,hp}$ are assumed as 10% and 80% of the fuel cell nominal power, as in [42]. Eventually, the fuel cell end-of-life occurs when the voltage degradation is 10%.

The battery degradation phenomena are highly specific to the cell type. Thus, it is difficult to generalize degradation models without experimental characterizations. Nevertheless, the number of equivalent charge/discharge cycles:

$$N_{bat} = \frac{\int |I_{bat}| dt}{2 Q_{bat,nom}}, \quad (18)$$

is considered as a rough indicator of the battery degradation. Some studies show that the battery life can reach up to 5000 equivalent cycles if the system is operated avoiding high C-rates, temperature peaks, full discharging, and overcharging [43–46]. Therefore, an important indicator is also the maximum battery temperature $T_{bat,max}$. Moreover, it is critical to control the battery charge, keeping it within a safe operating range. An indicator of the SoC control can be defined considering the deviation from a suitable reference as:

$$\varepsilon_{SoC} = SoC_{ref} - SoC. \quad (19)$$

Therefore, the standard deviation of ε_{SoC} can represent a suitable metric for the battery charge control, and it is denoted with $\sigma(\varepsilon_{SoC})$.

3. Adaptive and Predictive Energy Management System

Energy management refers to the control task of distributing the electric load demanded by the driver between the fuel cell and battery systems. This function is also called power-split, and it is a challenging aspect of hybrid vehicles because it involves multiple and contrasting targets, such as hydrogen consumption, fuel cell voltage degradation, maximum battery temperature, equivalent battery charge/discharge cycles, and SoC control.

This study adopts the energy management system developed in [31], which is divided into two stages as shown in Figure 5. When a new destination is inserted in the navigation system, the available route information is used for the optimal generation of predictive SoC and FCS power references. Afterward, when the drive starts, the references are used for the on-board power-split by an adaptive rule-based energy management strategy.

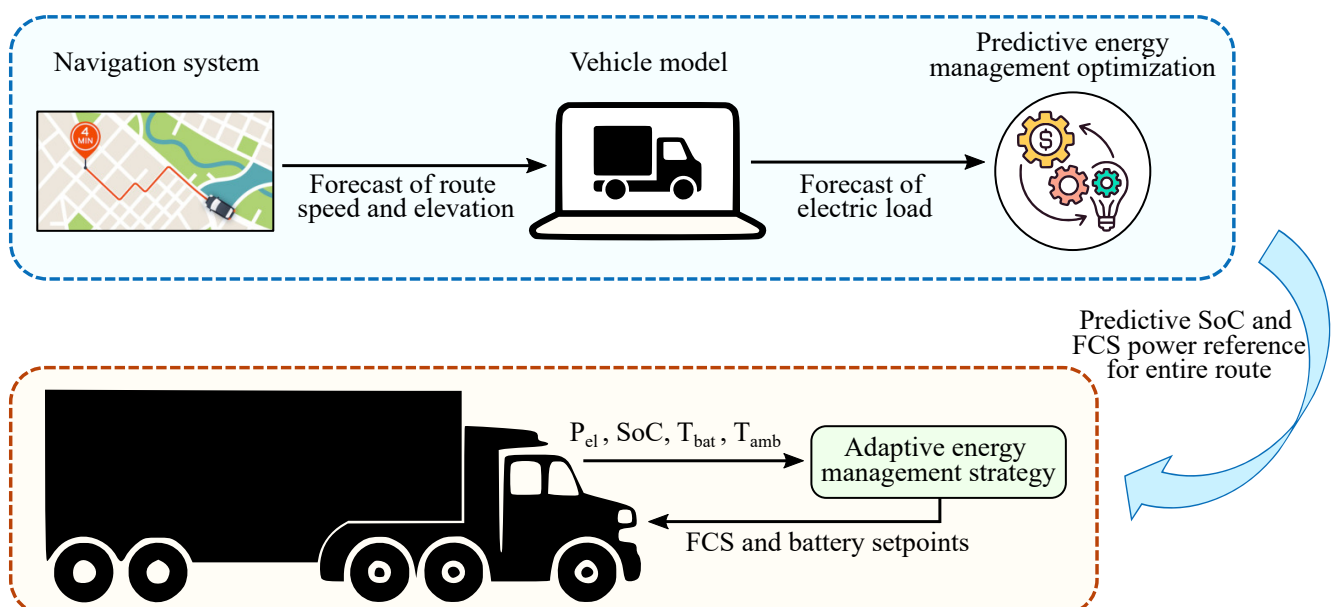


Figure 5. Control architecture of the predictive energy management system.

3.1. Optimal Generation of Predictive SoC and FCS Power References for Entire Route

Modern navigation systems can provide basic driving information of the route to the final destination, such as road elevation, curvature, speed limits, and traffic speed. This information can be used to forecast the electric load demand, allowing for predictive energy management optimization. For example, knowing that the fuel cell truck has to overcome a mountain, a predictive energy management system can ensure that the battery is sufficiently charged before the climb starts.

This work uses quadratic programming for the optimal generation of SoC and FCS power references with the following targets:

- maximize the fuel cell system efficiency,
- keep the SoC within the range 50–80%,
- and avoid fuel cell operation at high power.

The optimization method was developed in [31] to optimize the predictive SoC reference for the on-board energy management. On the other hand, the present work also uses the FCS power reference to increase the SoC control. Figure 6 shows the optimization results for the reference generation considering a driving cycle segment in which the fuel cell truck must overcome a hill. Before the climb starts at minute 20, the FCS is operated at maximum power to recharge the battery so that the long uphill will not cause a battery charge depletion beyond the defined constraint (i.e., 50%). Indeed, even if the FCS operates at maximum power between minutes 20 and 30, the battery charge goes from 80% to 50%. Therefore, the minimum SoC constraint would be violated if the battery was not fully charged before the climb.

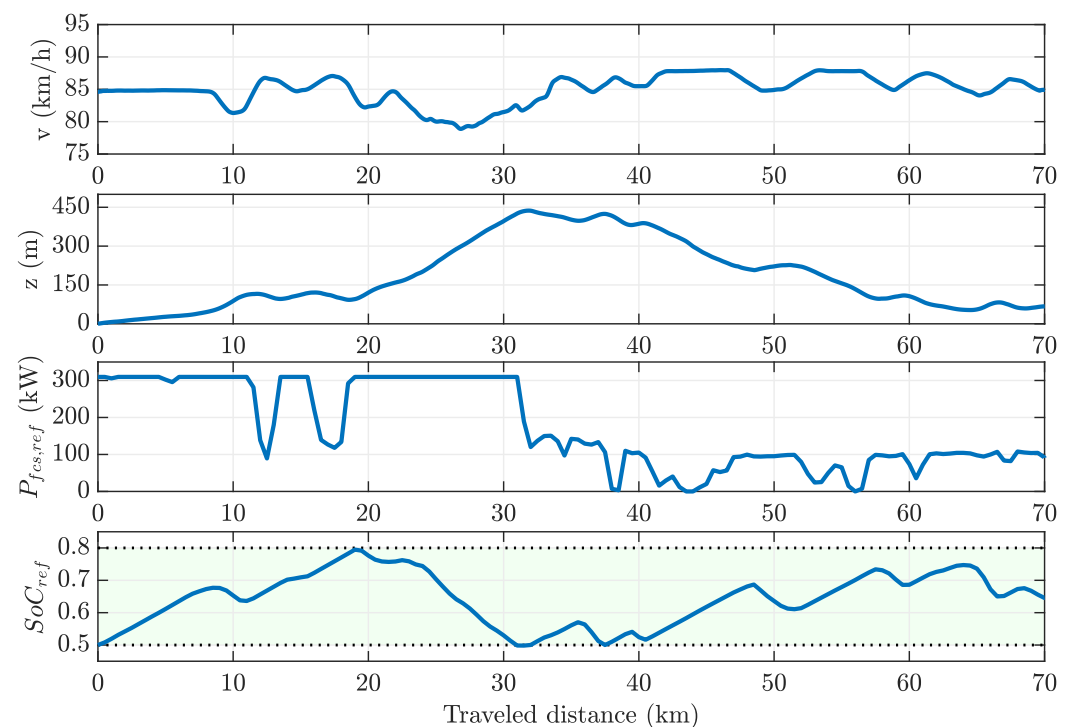


Figure 6. Optimal generation of predictive energy management references considering a driving cycle segment in which the fuel cell truck must overcome a hill. The figure shows speed, elevation, predictive FCS, and SoC references.

3.2. On-Board Adaptive Energy Management Strategy

The on-board energy management is performed by a rule-based control strategy, which is adaptive to the battery and ambient temperatures. The underlying idea is that in critical conditions, e.g., high temperatures, the battery usage is limited to allow its cooldown and avoid the degradation associated with temperatures peaks. The adaptive EMS is

implemented by properly adjusting the main control parameters to the current system state. The fuel cell power setpoint is denoted with $P_{fcs,set}$ and it is calculated as:

$$P_{fcs,set} = P_{fcs,ref} + r_1 \cdot (P_{el,des} - P_{fcs,ref}) + r_2 \cdot (SoC_{ref} - SoC) \tag{20}$$

$$\text{subject to: } |\dot{P}_{fcs,set}| < r_3 \tag{21}$$

$$\text{with: } r_1 = r_1(T_{bat}, T_{amb}), r_2 = r_2(T_{bat}, T_{amb}), r_3 = r_3(T_{bat}, T_{amb}) . \tag{22}$$

The first term on the right-hand side of (20) is the FCS power reference. The second one considers the deviation of the desired electric load $P_{el,des}$ from $P_{fcs,ref}$, whereas the third one the deviation of the SoC from the predictive reference. The rate of change of the setpoint is limited in (21) to reduce the fuel cell transient operation. The EMS parameters r_1 , r_2 , and r_3 are defined in (22) as function of the battery and ambient temperatures, making the strategy adaptive. On the other hand, the battery setpoint $P_{bat,set}$ is calculated as:

$$P_{bat,set} = P_{el,des} - P_{fcs} + P_{fcs,cool} + P_{bat,cool} , \tag{23}$$

compensating for the remaining part of the desired load and the electric losses of the cooling systems.

3.3. Optimal Calibration of EMS Parameters Using AVL CAMEO

The EMS calibration considers the multi-objective optimization of hydrogen consumption, fuel cell degradation, battery thermal state, equivalent charge/discharge cycles, and SoC control. This work uses AVL CAMEO to systematically vary the adaptive curve parameters to explore the trade-off between the key performance indicators (KPIs). Moreover, the Active DoE approach of CAMEO is adopted for optimal calibration, reducing process time and increasing accuracy. With a standard DoE approach (i.e., a pre-defined variation list), a lot of time and effort is wasted collecting data in areas out of interest while lacking measurements close to the Pareto fronts, which are crucial for optimal calibration. On the other hand, with Active DoE, CAMEO mainly focuses the experiments in the area of interest defined by the calibration targets. Figure 7 schematizes the working principle of the Active DoE approach. At every new measurement of vehicle performance, CAMEO creates models of the KPIs and uses them to define the variation parameters of the next test based on the optimization targets.

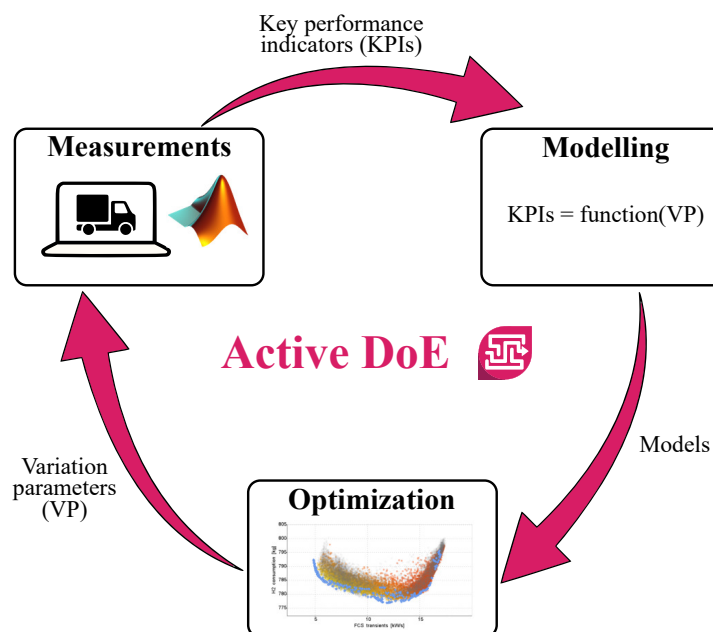


Figure 7. Representation of the Active DoE approach adopted by AVL CAMEO.

Finding a trade-off between five KPIs is a quite challenging and not straightforward task. Therefore, this work limits the trade-off analysis between the hydrogen consumption, m_{H_2} , and the fuel cell voltage degradation, ΔV_{fcs} . However, the following optimization constraints are imposed to guarantee sufficient battery life and SoC control:

$$N_{bat} < 1000 \text{ cycles}/100.000 \text{ km} , \quad (24)$$

$$T_{bat,max} < 47 \text{ }^\circ\text{C} , \quad (25)$$

$$\sigma(\varepsilon_{SoC}) < 0.03 . \quad (26)$$

4. Optimal Calibration Results

The optimal calibration process was ended after 700 evaluations of the KPIs over the 32 driving cycles, which required a relatively low simulation effort (i.e., 16 h using an office laptop). Figure 8 shows all the measurements collected during the calibration process. The blue markers indicate the measurements that meet all the calibration constraints (24)–(26), whereas the others do not. The red markers exceed the battery temperature constraint, the yellow ones the equivalent battery cycles constraint, and the green ones the SoC control constraint. The hydrogen consumption in Figure 8 has a relatively large range because related to different ambient temperatures, which affect the energy consumption of the fuel cell and battery cooling systems. The figure already shows that fuel cell degradation and battery equivalent cycles are contrasting targets, as the lowest degradation is obtained with parametrizations that exceeded the equivalent cycles constraint (yellow markers).

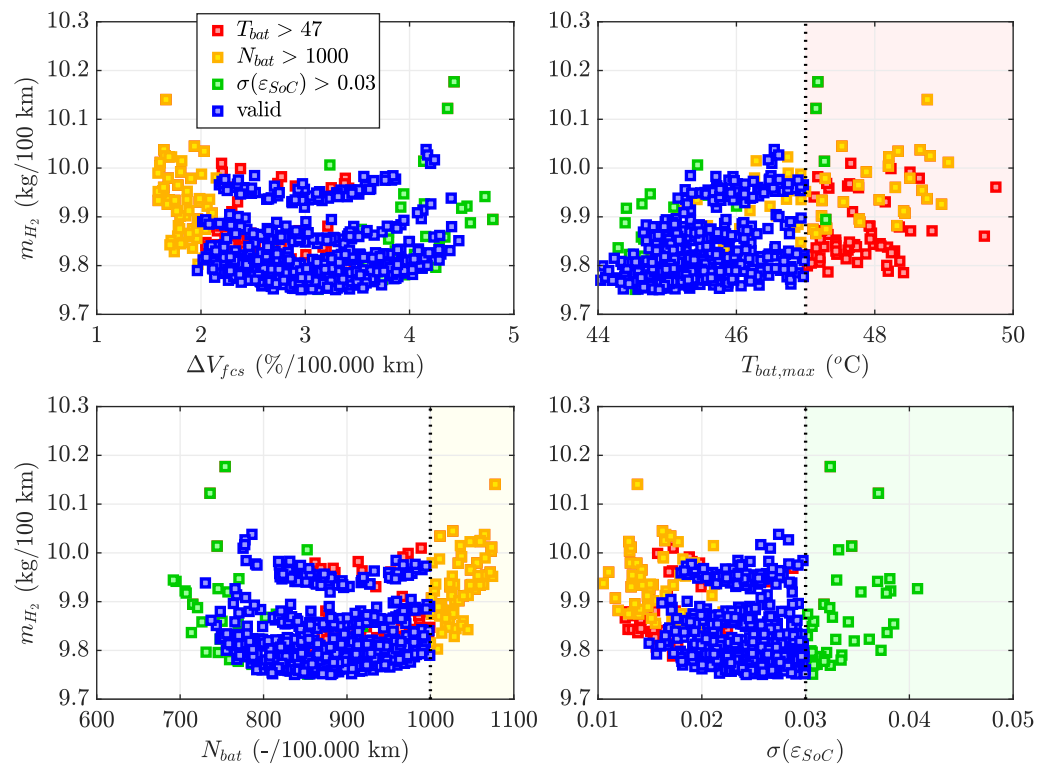


Figure 8. Measurements collected during the optimal calibration of the EMS parameters.

It is convenient to consider only the results related to a given ambient temperature to analyze the trade-offs between the performance indicators. Therefore, Figure 9 shows the valid measurements collected at $T_{amb} = 20 \text{ }^\circ\text{C}$, comparing hydrogen consumption, fuel cell degradation, and battery equivalent cycles. Here, the blue line delineates the Pareto front between the hydrogen consumption and voltage degradation. The green diamond marker identifies the optimal tuning of the EMS parameters, which is selected to find a good trade-off between the two targets based on the driving range and vehicle

lifetime requirements. Additionally, the figure shows an evident contrast between battery equivalent cycles and fuel cell degradation because if one power source is used less, the other needs to operate more to provide the electric load demand.

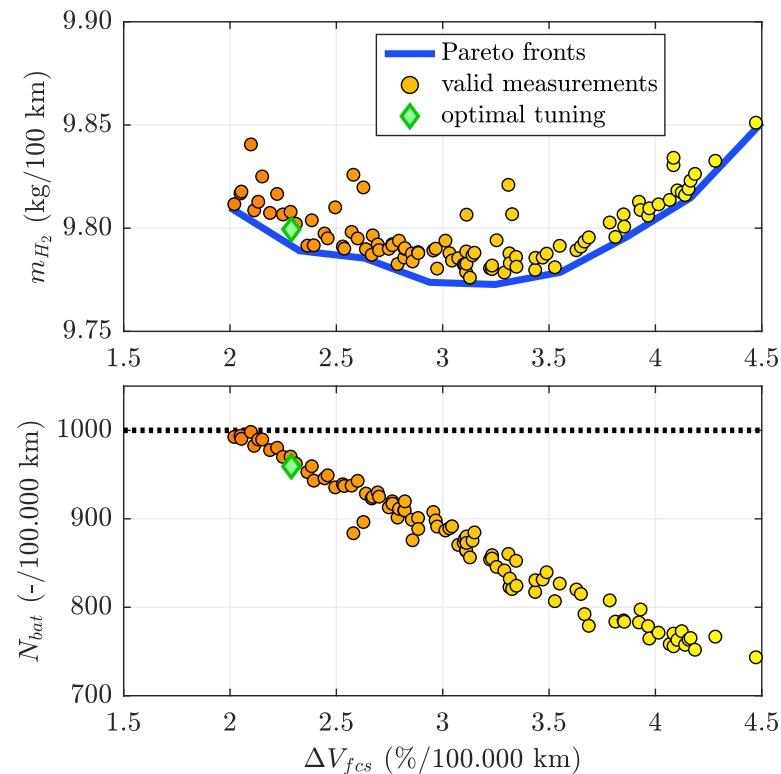


Figure 9. Trade-off between hydrogen consumption, fuel cell voltage degradation, and equivalent battery cycles. The figure shows only the valid measurements at $T_{amb} = 20\text{ }^{\circ}\text{C}$. The green marker corresponds to the selected optimal tuning.

Figure 10 shows the maps of the three EMS parameters resulting from the optimal calibration. It is evident that the battery temperature has a more dominant impact on the EMS parameters than the ambient one. In particular, the parameter r_1 increases with the battery temperature to limit its usage and allow the system to cool down. Indeed, if $r_1 = 1$, the EMS operates the FCS in load-follower mode resulting in limited battery usage. The power rate limit defined by r_3 increases at high temperatures to allow the FCS to follow the load demand.

Comparison with Non-Adaptive and Non-Predictive Strategies

The simulation results obtained with the optimized adaptive and predictive EMS are compared with those of non-adaptive and non-predictive strategies. For a fair comparison, the non-adaptive parameters are obtained from the optimal maps of Figure 10 at $T_{bat} = 35\text{ }^{\circ}\text{C}$ and $T_{amb} = 20\text{ }^{\circ}\text{C}$. The non-predictive strategy considers a constant SoC reference at 65% and a constant FCS power reference at its most efficient operating point (i.e., 55 kW). First, Figure 11 shows the comparison between adaptive and non-adaptive strategies, highlighting the evident benefits of avoiding temperature peaks. In normal conditions, the vehicle operation is identical. However, the adaptive EMS reduces the battery usage at minute 110 to cool down the system, avoiding the temperature peak. The impact on the maximum battery temperature is significant ($45\text{ }^{\circ}\text{C}$ versus $50\text{ }^{\circ}\text{C}$), even though the power-split only presents small differences. On the other hand, the impact on hydrogen consumption is negligible, but the fuel cell voltage degradation is slightly increased. It should be noted that the speed profiles in both simulations are the same because the EMS ensures that the load demand is always provided by the fuel cell and battery systems.

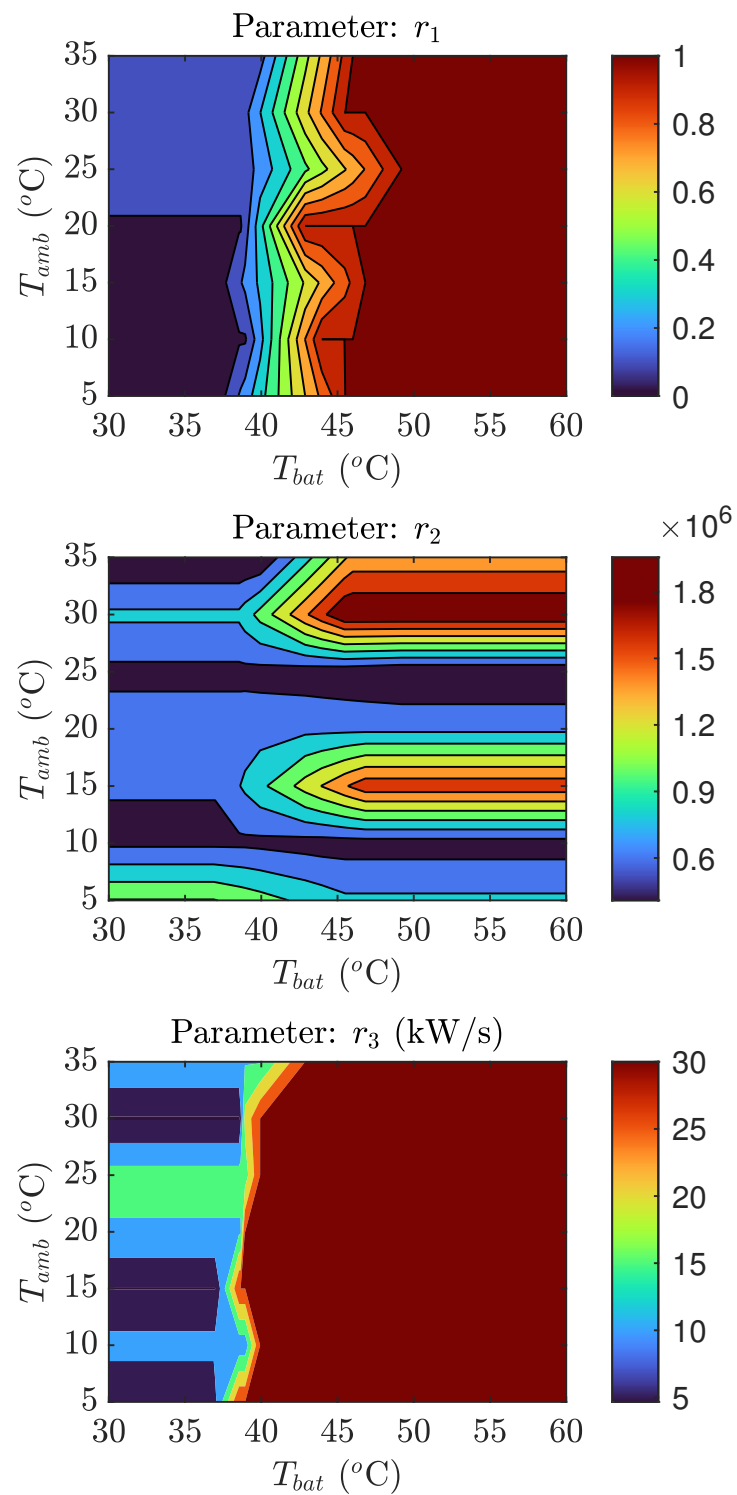


Figure 10. Adaptive EMS parameters resulting from the optimal calibration process. Each parameter is mapped against ambient and battery temperature.

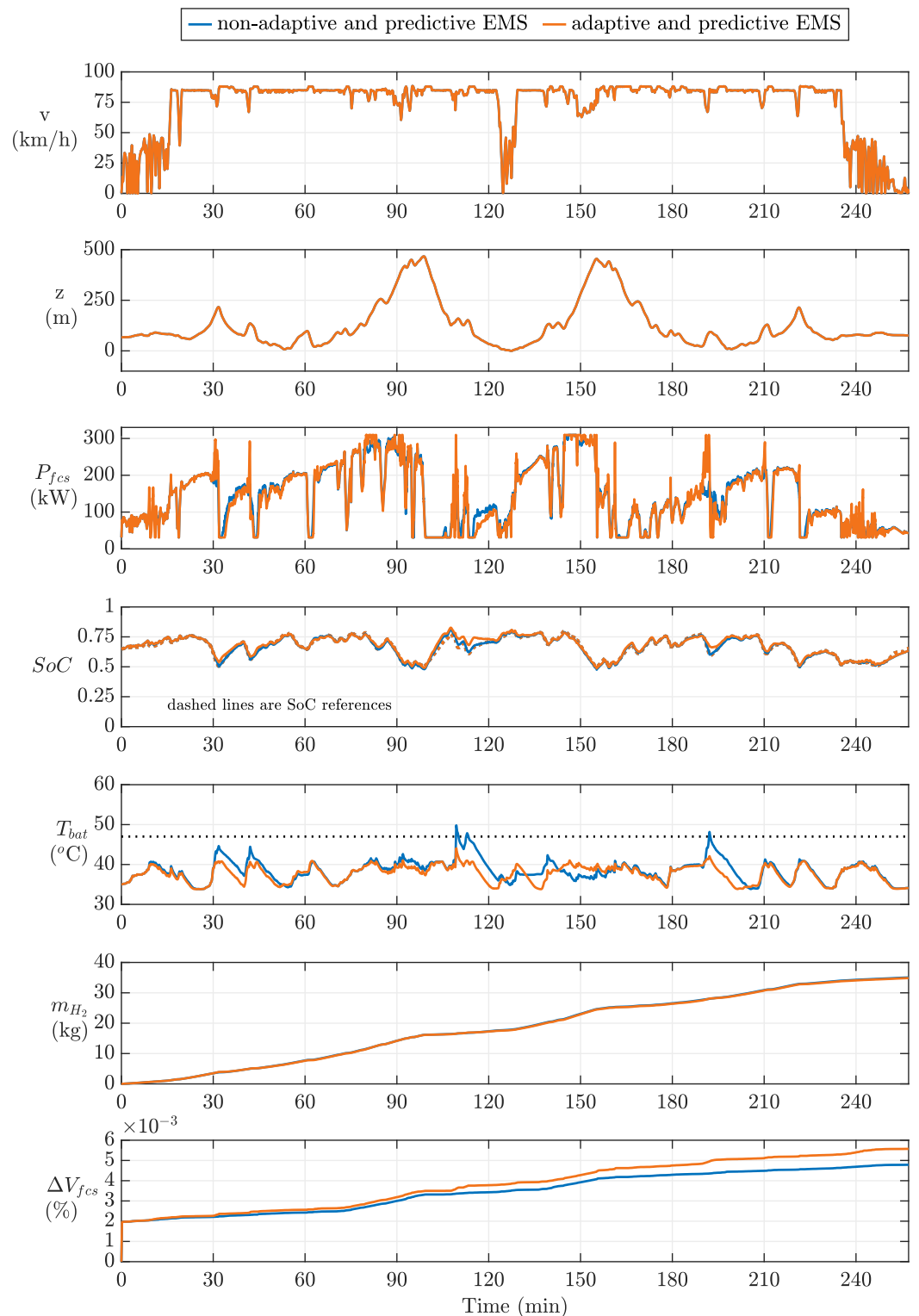


Figure 11. Simulation results comparison between adaptive and non-adaptive EMSs in terms of speed, elevation, fuel cell system power, state of charge, battery temperature, hydrogen consumption, and fuel cell voltage degradation. The ambient temperature is 20 °C.

Figure 12 shows the benefits of using a predictive EMS compared to a non-predictive one. In this case, the two strategies determine a significant difference in the vehicle operation. In particular, the predictive EMS reduces the fuel cell operation at high power to increase the fuel cell efficiency and reduce fuel cell degradation. Moreover, the SoC is significantly closer to the reference, meaning that a better control of the battery charge is

achieved. Indeed, in this driving cycle, the predictive EMS yields a depth of discharge of 34%, whereas the non-predictive yields one of 59%. Therefore, it can be expected that there is a substantial benefit in limiting accelerated degradation by operating the battery with the desired depth of discharge avoiding critical discharges.

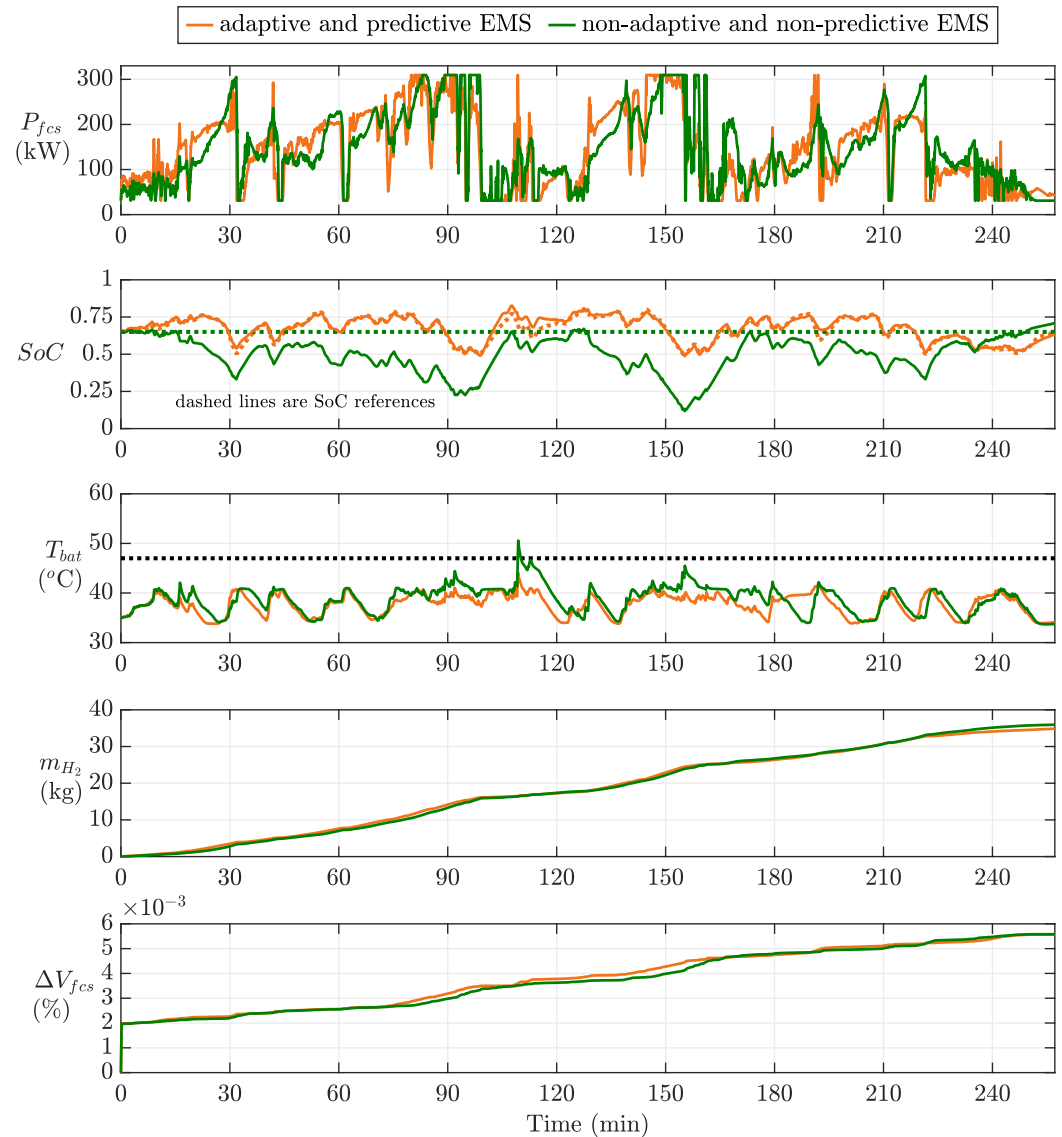


Figure 12. Simulation results comparison between predictive and non-predictive EMSs at ambient temperature of 20 °C.

Table 1 lists the KPIs related to the simulation results of Figures 11 and 12 to provide a quantitative understanding in relation to the signals depicted in the figures.

Table 1. Comparison of KPIs for the specific driving cycle under investigation at $T_{amb} = 20$ °C.

EMS		m_{H_2} (kg/100 km)	ΔV_{fcs} (%/100.000 km)	N_{bat} (–/100.000 km)	$T_{bat,max}$ (°C)	$\sigma(\epsilon_{SoC})$
Adap.	Pred.					
Yes	Yes	11.06	1.77	965	44.1	0.0181
No	Yes	11.12	1.52	1040	49.8	0.0105
No	No	11.34	1.77	1130	50.6	0.1220

Lastly, Figure 13 shows the global KPIs calculated for the sequence of 32 cycles at different ambient temperatures. In general, the hydrogen consumption increases with

the ambient temperature due to the higher energy consumption of the cooling systems. As expected, the adaptive EMS results in higher fuel cell voltage degradation because it shifts the transients loads to the FCS, allowing the battery to cool down. Consequently, the equivalent battery cycles are reduced compared to the other strategies. Eventually, only the adaptive EMS can meet all the constraints assigned for equivalent battery cycles, maximum battery temperature, and SoC control for all ambient temperatures.

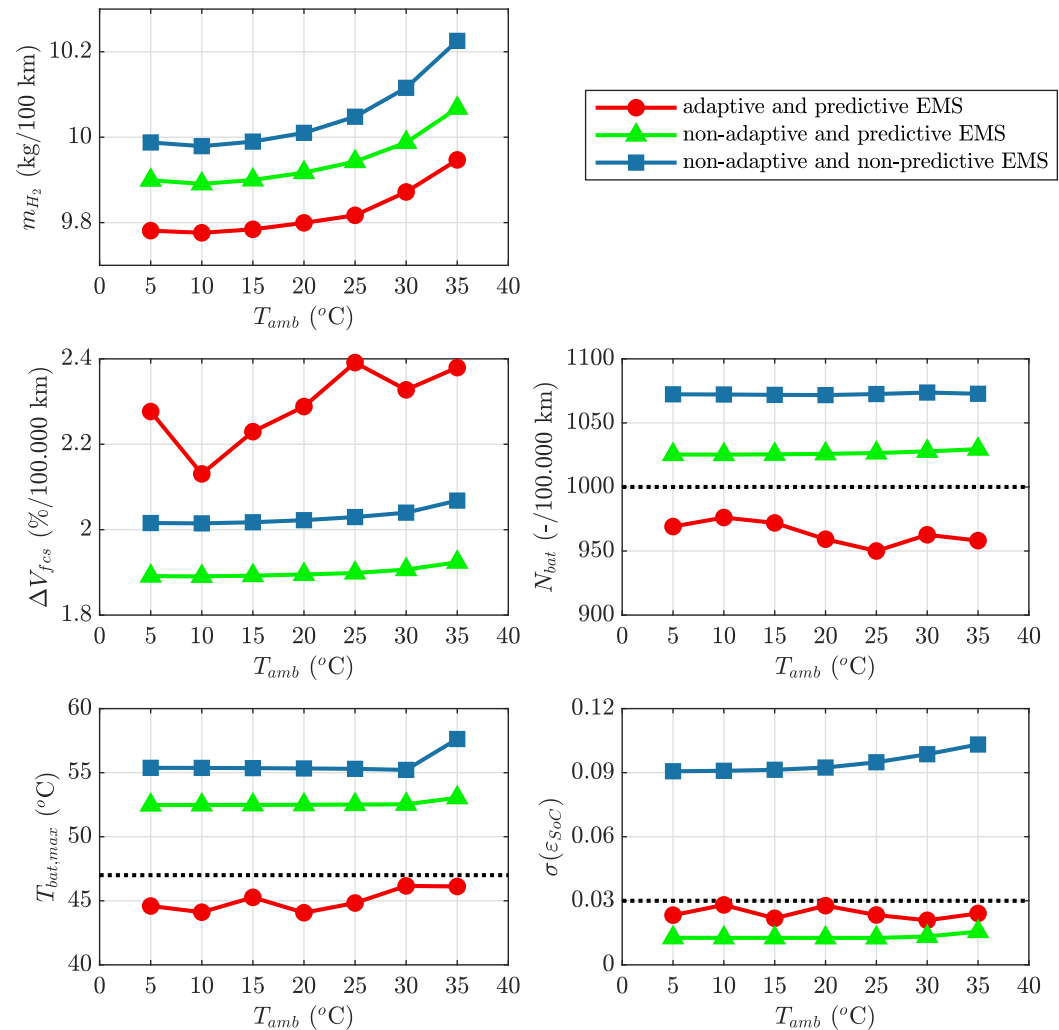


Figure 13. Comparison of KPIs between the adaptive and predictive EMS versus the non-adaptive and non-predictive strategies at different ambient temperatures.

5. Conclusions

This paper proposed an adaptive and predictive energy management strategy for fuel cell electric trucks to exploit the interaction between energy and thermal management. In particular, the control strategy is adaptive to the battery and ambient temperatures to ensure that, in critical conditions, the battery usage is limited to avoid temperature peaks. The maps of the adaptive EMS parameters were designed and optimally tuned using AVL CAMEO considering hydrogen consumption, fuel cell degradation, battery thermal state, equivalent charge/discharge cycles, and SoC control.

The simulations show that using the adaptive EMS determines small changes in the power-split but significantly impacts the battery temperature peaks. Moreover, the strategies comparison highlights the benefits of predictive energy management for SoC control and hydrogen consumption for fuel cell trucks driving mountain/hilly routes. Eventually, the optimal calibration using AVL CAMEO yield a robust EMS design, meeting all the optimization targets and constraints.

Future investigations can consider the design of energy management strategies that are adaptive to additional parameters, such as vehicle weight, state-of-health of the fuel cell, and battery systems. The complexity of the design and calibration of the adaptive EMS parameters maps would significantly increase. However, using AVL CAMEO would be a solution to systematically and efficiently (using Active DoE) explore the design space of the control parameters.

Author Contributions: Conceptualization, A.F., H.-M.K. and C.H.; methodology, A.F.; software, A.F., S.Z., H.-M.K., S.G., M.H. and J.P.; validation, A.F., S.Z., H.-M.K., S.G., M.H. and J.P.; formal analysis, A.F.; investigation, A.F.; resources, C.H.; data curation, A.F.; writing—original draft preparation, A.F. and C.H.; writing—review and editing, A.F., S.Z., H.-M.K., S.G., M.H., J.P. and C.H.; visualization, A.F.; supervision, A.F.; project administration, C.H.; funding acquisition, C.H. All authors have read and agreed to the published version of the manuscript.

Funding: The financial support by the Austrian Federal Ministry for Digital and Economic Affairs, the National Foundation for Research, Technology and Development, and the Christian Doppler Research Association is gratefully acknowledged. This work has been created in cooperation with the Austrian research projects “HyTruck” (grant no. 868790) and “FC4HD” (grant no. 885044). Open Access Funding by TU Wien.

Institutional Review Board Statement: Not applicable.

Informed Consent Statement: Not applicable.

Conflicts of Interest: The authors declare no conflict of interest. The funders had no role in the design of the study; in the collection, analyses, or interpretation of data; in the writing of the manuscript, or in the decision to publish the results.

Nomenclature

The following nomenclature is used in the paper:

$P_{el,des}$	Desired electric load
α	Road slope
v	Vehicle speed
v_{des}	Desired vehicle speed
P_{el}	Electric load
P_{fcs}	Fuel cell power
P_{bat}	Battery power
$P_{fcs,cool}$	Electric losses of fuel cell cooling system
$P_{bat,cool}$	Electric losses of battery cooling system
$P_{fcs,nom}$	Nominal fuel cell power
\dot{P}_{fcs}	Rate of change of fuel cell power
$P_{bat,min}$	Minimum battery power
$P_{bat,max}$	Maximum battery power
SoC	Battery state of charge
T_{bat}	Battery temperature
\dot{SoC}	Rate of change of battery state of charge
V_{oc}	Battery open circuit voltage
R_{int}	Battery internal resistance
$Q_{bat,nom}$	Nominal battery charge
T_{amb}	Ambient temperature
\dot{Q}_{chill}	Cooling power of chiller system
COP	Coefficient of performance of battery cooling system
P_m	Electric motor power
P_{aux}	Electric power of external auxiliary systems
P_w	Mechanical power at wheels
P_{br}	Mechanical braking power
F_{res}	Resistant force to vehicle motion
m_v	Vehicle mass

m_{H_2}	Hydrogen consumption
\dot{m}_{H_2}	Hydrogen consumption rate
ΔV_{fcs}	Fuel cell voltage degradation
$\Delta V_{fcs,ss}$	Share of fuel cell voltage degradation caused by start-up/shut-down cycles
$\Delta V_{fcs,lp}$	Share of fuel cell voltage degradation caused by low-power operation
$\Delta V_{fcs,hp}$	Share of fuel cell voltage degradation caused by high-power operation
$\Delta V_{fcs,dl}$	Share of fuel cell voltage degradation caused by dynamic loading
$N_{fcs,starts}$	Number of fuel cell starts
$t_{fcs,lp}$	Time at low-power operation
$t_{fcs,hp}$	Time at high-power operation
N_{bat}	Number of equivalent charge/discharge cycles
I_{bat}	Battery current
ε_{SoC}	Deviation from SoC reference
SoC_{ref}	Predictive SoC reference
$\sigma(\varepsilon_{SoC})$	Standard deviation of ε_{SoC}
$P_{fcs,set}$	Fuel cell power setpoint
$P_{fcs,ref}$	Predictive fuel cell power reference
$\dot{P}_{fcs,set}$	Rate of change of fuel cell power setpoint
r_1	EMS parameter 1
r_2	EMS parameter 2
r_3	EMS parameter 3
$P_{bat,set}$	Battery power setpoint
$T_{bat,max}$	Maximum battery temperature

References

- Lee, D.Y.; Elgowainy, A.; Kotz, A.; Vijayagopal, R.; Marcinkoski, J. Life-cycle implications of hydrogen fuel cell electric vehicle technology for medium- and heavy-duty trucks. *J. Power Sources* **2018**, *393*, 217–229. [\[CrossRef\]](#)
- Kast, J.; Vijayagopal, R.; Gangloff, J.J.; Marcinkoski, J. Clean commercial transportation: Medium and heavy duty fuel cell electric trucks. *Int. J. Hydrogen Energy* **2017**, *42*, 4508–4517. [\[CrossRef\]](#)
- Liu, F.; Zhao, F.; Liu, Z.; Hao, H. The impact of fuel cell vehicle deployment on road transport greenhouse gas emissions: The China case. *Int. J. Hydrogen Energy* **2018**, *43*, 22604–22621. [\[CrossRef\]](#)
- Kast, J.; Morrison, G.; Gangloff, J.J.; Vijayagopal, R.; Marcinkoski, J. Designing hydrogen fuel cell electric trucks in a diverse medium and heavy duty market. *Res. Transp. Econ.* **2018**, *70*, 139–147. [\[CrossRef\]](#)
- Ferrara, A.; Okoli, M.; Jakubek, S.; Hametner, C. Energy Management of Heavy-Duty Fuel Cell Electric Vehicles: Model Predictive Control for Fuel Consumption and Lifetime Optimization. *IFAC-PapersOnLine* **2020**, *53*, 14205–14210. [\[CrossRef\]](#)
- Enang, W.; Bannister, C. Modelling and control of hybrid electric vehicles (A comprehensive review). *Renew. Sustain. Energy Rev.* **2017**, *74*, 1210–1239. [\[CrossRef\]](#)
- Lü, X.; Wu, Y.; Lian, J.; Zhang, Y.; Chen, C.; Wang, P.; Meng, L. Energy management of hybrid electric vehicles: A review of energy optimization of fuel cell hybrid power system based on genetic algorithm. *Energy Convers. Manag.* **2020**, *205*, 112474. [\[CrossRef\]](#)
- Kasimalla, V.K.; G., N.S.; Velisala, V. A review on energy allocation of fuel cell/battery/ultracapacitor for hybrid electric vehicles. *Int. J. Energy Res.* **2018**, *42*, 4263–4283. [\[CrossRef\]](#)
- Ferrara, A.; Hametner, C. Rule-Based Energy Management Strategy of Fuel Cell/Ultracapacitor/Battery Vehicles: Winner of the IEEE VTS Motor Vehicles Challenge 2020. In Proceedings of the 2020 IEEE Vehicle Power and Propulsion Conference (VPPC), Gijon, Spain, 18 November–16 December 2020. [\[CrossRef\]](#)
- Ravey, A.; Blunier, B.; Miraoui, A. Control Strategies for Fuel-Cell-Based Hybrid Electric Vehicles: From Offline to Online and Experimental Results. *IEEE Trans. Veh. Technol.* **2012**, *61*, 2452–2457. [\[CrossRef\]](#)
- Ettihir, K.; Boulon, L.; Agbossou, K. Optimization-based energy management strategy for a fuel cell/battery hybrid power system. *Appl. Energy* **2016**, *163*, 142–153. [\[CrossRef\]](#)
- Fletcher, T.; Thring, R.; Watkinson, M. An Energy Management Strategy to concurrently optimise fuel consumption & PEM fuel cell lifetime in a hybrid vehicle. *Int. J. Hydrogen Energy* **2016**, *41*, 21503–21515. [\[CrossRef\]](#)
- Kemper, P.; Rehlaender, P.; Witkowski, U.; Schwung, A. Competitive Evaluation of Energy Management Strategies for Hybrid Electric Vehicle Based on Real World Driving. In Proceedings of the 2017 European Modelling Symposium (EMS), Manchester, UK, 20–21 November 2017; pp. 151–156. [\[CrossRef\]](#)
- Zhou, D.; Ravey, A.; Al-Durra, A.; Gao, F. A comparative study of extremum seeking methods applied to online energy management strategy of fuel cell hybrid electric vehicles. *Energy Convers. Manag.* **2017**, *151*, 778–790. [\[CrossRef\]](#)
- Song, K.; Chen, H.; Wen, P.; Zhang, T.; Zhang, B.; Zhang, T. A comprehensive evaluation framework to evaluate energy management strategies of fuel cell electric vehicles. *Electrochim. Acta* **2018**, *292*, 960–973. [\[CrossRef\]](#)

16. Li, X.; Wang, Y.; Yang, D.; Chen, Z. Adaptive energy management strategy for fuel cell/battery hybrid vehicles using Pontryagin's Minimal Principle. *J. Power Sources* **2019**, *440*, 227105. [[CrossRef](#)]
17. Simmons, K.; Guezennec, Y.; Onori, S. Modeling and energy management control design for a fuel cell hybrid passenger bus. *J. Power Sources* **2014**, *246*, 736–746. [[CrossRef](#)]
18. Geng, C.; Jin, X.; Zhang, X. Simulation research on a novel control strategy for fuel cell extended-range vehicles. *Int. J. Hydrogen Energy* **2019**, *44*, 408–420. [[CrossRef](#)]
19. Guo, Q.; Zhao, Z.; Shen, P.; Zhou, P. Optimization management of hybrid energy source of fuel cell truck based on model predictive control using traffic light information. *Control. Theory Technol.* **2019**, *17*, 309–324. [[CrossRef](#)]
20. Hu, X.; Zou, C.; Tang, X.; Liu, T.; Hu, L. Cost-Optimal Energy Management of Hybrid Electric Vehicles Using Fuel Cell/Battery Health-Aware Predictive Control. *IEEE Trans. Power Electron.* **2020**, *35*, 382–392. [[CrossRef](#)]
21. Wu, J.; Zhang, N.; Tan, D.; Chang, J.; Shi, W. A robust online energy management strategy for fuel cell/battery hybrid electric vehicles. *Int. J. Hydrogen Energy* **2020**, *45*, 14093–14107. [[CrossRef](#)]
22. Sun, Y.; Xia, C.; Yin, B.; Gao, H.; Han, J.; Liu, J. Energy management strategy for FCEV considering degradation of fuel cell. *Int. J. Green Energy* **2022**, 1–12. [[CrossRef](#)]
23. Zhang, Y.; Ma, R.; Zhao, D.; Huangfu, Y.; Liu, W. A Novel Energy Management Strategy Based on Dual Reward Function Q-learning for Fuel Cell Hybrid Electric Vehicle. *IEEE Trans. Ind. Electron.* **2022**, *69*, 1537–1547. [[CrossRef](#)]
24. Min, D.; Song, Z.; Chen, H.; Wang, T.; Zhang, T. Genetic algorithm optimized neural network based fuel cell hybrid electric vehicle energy management strategy under start-stop condition. *Appl. Energy* **2022**, *306*, 118036. [[CrossRef](#)]
25. Deng, K.; Liu, Y.; Hai, D.; Peng, H.; Löwenstein, L.; Pischinger, S.; Hameyer, K. Deep reinforcement learning based energy management strategy of fuel cell hybrid railway vehicles considering fuel cell aging. *Energy Convers. Manag.* **2022**, *251*, 115030. [[CrossRef](#)]
26. Barelli, L.; Bidini, G.; Ciupăgeanu, D.; Pianese, C.; Polverino, P.; Sorrentino, M. Stochastic power management approach for a hybrid solid oxide fuel cell/battery auxiliary power unit for heavy duty vehicle applications. *Energy Convers. Manag.* **2020**, *221*, 113197. [[CrossRef](#)]
27. Ilio, G.D.; Giorgio, P.D.; Tribioli, L.; Bella, G.; Jannelli, E. Preliminary design of a fuel cell/battery hybrid powertrain for a heavy-duty yard truck for port logistics. *Energy Convers. Manag.* **2021**, *243*, 114423. [[CrossRef](#)]
28. Feng, Y.; Dong, Z. Optimal energy management with balanced fuel economy and battery life for large hybrid electric mining truck. *J. Power Sources* **2020**, *454*, 227948. [[CrossRef](#)]
29. Wu, X.; Hu, X.; Yin, X.; Peng, Y.; Pickert, V. Convex programming improved online power management in a range extended fuel cell electric truck. *J. Power Sources* **2020**, *476*, 228642. [[CrossRef](#)]
30. Feng, Y.; Dong, Z. Integrated design and control optimization of fuel cell hybrid mining truck with minimized lifecycle cost. *Appl. Energy* **2020**, *270*, 115164. [[CrossRef](#)]
31. Zendegan, S.; Ferrara, A.; Jakubek, S.; Hametner, C. Predictive Battery State of Charge Reference Generation Using Basic Route Information for Optimal Energy Management of Heavy-Duty Fuel Cell Vehicles. *IEEE Trans. Veh. Technol.* **2021**, *70*, 12517–12528. [[CrossRef](#)]
32. Ferrara, A.; Jakubek, S.; Hametner, C. Energy management of heavy-duty fuel cell vehicles in real-world driving scenarios: Robust design of strategies to maximize the hydrogen economy and system lifetime. *Energy Convers. Manag.* **2021**, *232*, 113795. [[CrossRef](#)]
33. Padovani, T.M.; Debert, M.; Colin, G.; Chamaillard, Y. Optimal Energy Management Strategy including Battery Health through Thermal Management for Hybrid Vehicles. *IFAC Proc. Vol.* **2013**, *46*, 384–389. [[CrossRef](#)]
34. Amini, M.R.; Sun, J.; Kolmanovsky, I. Two-Layer Model Predictive Battery Thermal and Energy Management Optimization for Connected and Automated Electric Vehicles. In Proceedings of the 2018 IEEE Conference on Decision and Control (CDC), Miami, FL, USA, 17–19 December 2018. [[CrossRef](#)]
35. Wang, Y.; Gao, Q.; Wang, G.; Lu, P.; Zhao, M.; Bao, W. A review on research status and key technologies of battery thermal management and its enhanced safety. *Int. J. Energy Res.* **2018**, *42*, 4008–4033. [[CrossRef](#)]
36. Wu, W.; Wang, S.; Wu, W.; Chen, K.; Hong, S.; Lai, Y. A critical review of battery thermal performance and liquid based battery thermal management. *Energy Convers. Manag.* **2019**, *182*, 262–281. [[CrossRef](#)]
37. Liu, H.; Wei, Z.; He, W.; Zhao, J. Thermal issues about Li-ion batteries and recent progress in battery thermal management systems: A review. *Energy Convers. Manag.* **2017**, *150*, 304–330. [[CrossRef](#)]
38. Hydrogen Truck Austria, H. Project Founded by the Austrian Research Promotion Agency (FFG). 2019. Available online: <https://www.wiva.at/v2/portfolio-item/hydrogen-truck-austria/> (accessed on 20 January 2022).
39. Heavy-Duty Fuel Cell Road Demonstrator, F. Project Founded by the Austrian Research Promotion Agency (FFG). 2021. Available online: <https://www.klimafonds.gv.at/themen/mobilitaetswende/serviceseiten/zem/fc4hd-heavy-duty-fuel-cell-road-demonstrator/> (accessed on 20 January 2022).
40. Mohan, G.; Assadian, F.; Longo, S. Comparative analysis of forward-facing models vs backward-facing models in powertrain component sizing. In Proceedings of the Hybrid and Electric Vehicles Conference 2013 (HEVC 2013), Institution of Engineering and Technology, London, UK, 6–7 November 2013. [[CrossRef](#)]
41. Pei, P.; Chang, Q.; Tang, T. A quick evaluating method for automotive fuel cell lifetime. *Int. J. Hydrogen Energy* **2008**, *33*, 3829–3836. [[CrossRef](#)]

42. Ferrara, A.; Hametner, C. Impact of Energy Management Strategies on Hydrogen Consumption and Start-up/Shut-down Cycles in Fuel Cell-Ultracapacitor-Battery Vehicles. *IEEE Trans. Veh. Technol.* **2021**, *1*. [[CrossRef](#)]
43. Haidl, P.; Buchroithner, A.; Schweighofer, B.; Bader, M.; Wegleiter, H. Lifetime Analysis of Energy Storage Systems for Sustainable Transportation. *Sustainability* **2019**, *11*, 6731. [[CrossRef](#)]
44. Hesse, H.; Schimpe, M.; Kucevic, D.; Jossen, A. Lithium-Ion Battery Storage for the Grid—A Review of Stationary Battery Storage System Design Tailored for Applications in Modern Power Grids. *Energies* **2017**, *10*, 2107. [[CrossRef](#)]
45. Han, X.; Lu, L.; Zheng, Y.; Feng, X.; Li, Z.; Li, J.; Ouyang, M. A review on the key issues of the lithium ion battery degradation among the whole life cycle. *eTransportation* **2019**, *1*, 100005. [[CrossRef](#)]
46. Rechargeable Batteries. In *Batteries for Portable Devices*; Elsevier: Amsterdam, The Netherlands, 2005; p. 135. [[CrossRef](#)]